Journal Pre-proof

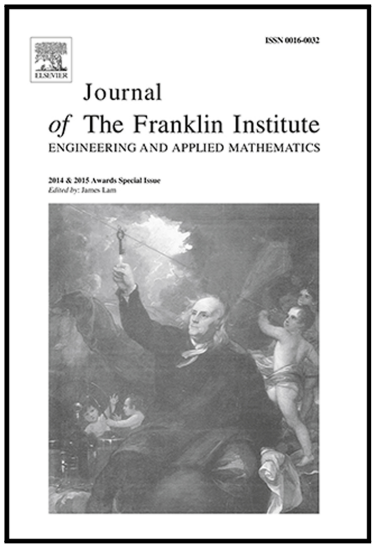

Event-triggered zeroing dynamics for motion control of Stewart platform

Yunong Zhang, Huanchang Huang, Shuai Li, Jian Li, Liangyu He

PII: S0016-0032(20)30164-2
DOI: https://doi.org/10.1016/j.jfranklin.2020.02.060
Reference: FI 4479

To appear in: *Journal of the Franklin Institute*

Received date: 25 January 2019
Revised date: 25 December 2019
Accepted date: 29 February 2020

Please cite this article as: Yunong Zhang, Huanchang Huang, Shuai Li, Jian Li, Liangyu He, Event-triggered zeroing dynamics for motion control of Stewart platform, *Journal of the Franklin Institute* (2020), doi: https://doi.org/10.1016/j.jfranklin.2020.02.060

Event-triggered zeroing dynamics for motion control of Stewart platform

Yunong Zhang[a], Huanchang Huang[a], Shuai Li[b,*], Jian Li[a], Liangyu He[a]

[a] *School of Information Science and Technology, Sun Yat-sen University, Guangzhou 510006, China*
[b] *College of Engineering, Swansea University, Swansea, Wales, sa17en, UK*

Abstract

Zeroing dynamics (ZD) was originally proposed and investigated for solving time-varying problems. Due to its advantages in convergence and accuracy, ZD has been successfully extended to various areas, including automatic control, robotics and numerical computation. In this paper, we further propose a novel one called event-triggered zeroing dynamics (ETZD) by incorporating the event-triggered strategy to improve the practicability of ZD. Absorbing the advantages of event-triggered strategy, ETZD can not only significantly reduce the consumption on computation but also maintain the original advantages of ZD. For better understanding, we employ ETZD to design a specific motion controller of a popular type of robot manipulators (i.e., Stewart platform). The stability of the motion controller is presented and analyzed via Lyapunov analysis. Furthermore, two different shaped path tracking tasks are executed in numerical experiments, and compared with conventional ZD controllers, to illustrate the advantage in convergence, accuracy and practicability of ETZD controller.

Keywords: Zeroing dynamics, Event-triggered strategy, Motion control, Stewart platform, Simulative experiments

[☆]This work is supported by the National Natural Science Foundation of China (with numbers 61473323 and 61401385), by the Laboratory Open Fund of Sun Yat-sen University (with number 20160209).

[*]Corresponding author.
E-mail Address: shuaili@ieee.org

1. Introduction

In scientific researches and practical production, time-varying problems appear frequently as difficulties. To solve them, many powerful methods have been proposed and investigated. Among numerous methods, zeroing dynamics (ZD, also termed, zeroing neural network, ZNN), which is essentially proposed for time-varying problems, is an effective alternative [1, 2, 3, 4, 5]. Conventionally, the main idea of ZD is using a design formula to zero out an error function, which is chosen according to the optimization objective of the target time-varying problem [1, 2]. For example, given the desired result $y_{\mathrm{d}}(t)$ and the actual result $y_{\mathrm{a}}(t)$, an error function $e(t) = y_{\mathrm{d}}(t) - y_{\mathrm{a}}(t)$ can be forced to zero by applying the ZD design formula $\dot{e}(t) = -\lambda e(t)$. Note that, with parameter $\lambda > 0$, the ZD design formula guarantees that $\mathbf{e}(t)$ converges to zero exponentially. Consequently, by substituting specific parts of the target problem into the ZD design formula, a dynamic solution model, which uses time-derivative information, can be derived.

Nowadays, ZD has successfully found its application in different situations with advantages in convergence and accuracy. For example, in [4], Petkovic et al. utilized ZD to develop solution models for matrix inversion and pseudoinversion. The problem of time-varying matrix square root finding was solved by Xiao with finite-time ZD method [5]. Note that the conventional method (i.e., Newton iteration) is found to be one special case in this modeling framework [4, 6, 7].

To broaden the scope of application of ZD method, it has been improved by combining with different methods. Thereinto, two hybrid methods, i.e., zeroing gradient (ZG) dynamics and zeroing quadratic programming, have successfully dealt with some difficulties on different control systems [8, 9, 10, 11]. ZG dynamics, which combines ZD with gradient descent, has the ability to achieve satisfactory control accuracy in systems with singularities, e.g., IPC (inverted pendulum on a cart) system [8] and chaotic systems [9]. The singularity-conquering ability makes ZD more practical and attractive in applications. By using zeroing quadratic programming, which combines ZD and Lagrange duality to solve quadratic programs, several motion control schemes are proposed and investigated for the control of redundant robot manipulators [12, 13, 14]. Due to the incorporation of quadratic programming (QP), these schemes can deal with inequality constraints and equality constraints, which extends the application horizon of ZD. For example, this type of hybrid scheme has found successful solutions

in different applications for serial redundant robot manipulators in terms of robust control and obstacle avoidance [12, 14].

Inspired by the above two hybrid methods, we make progress along this direction and attempt to combine ZD and the event-triggered strategy to propose the first event-triggered zeroing dynamics (ETZD). This novel design aims to improve the practicability of ZD by reducing the consumption on computation and data transmission largely, while maintain the original advantages of ZD.

In recent years, to reduce the consumption on computation and transmission, event-triggered control scheme has attracted a lot of attention [15, 16, 17, 18, 19, 20, 21]. Compared with conventional periodic control, event-triggered control only does the computation and transmission for the system when the feedback error grows beyond a threshold (or say, event-triggered function). This measure has been adopted by numerous researchers. For example, Fan and Yang proposed an event-triggered control scheme for the observer-based output feedback control problems [19], reducing the frequency of the communication between sensors and the control unit. Besides, the event triggering technique was adopted to deal with the problem of synchronizing delayed neural networks by Pradeep et al. in [20]. As for complex control problem like spacecraft attitude control, Wang et al. designed a controller with event triggering mechanism for attitude stabilization of spacecraft with or without presents of disturbance [21].

Thus, it is worthy of exploration for the integration of event-triggered strategy in ZD to improve the practicability of ZD by reducing the consumption on computation and transmission.

Robotic systems have attracted the attention of numerous researchers due to their potential efficiency in industrial applications. Many researchers have devoted a significant amount of effort to improve the practicability of robotic systems including manipulators [22, 23, 24, 25, 26]. As a class of manipulators, parallel manipulators are popular with advantages of small inertia, small position error, high stiffness, high capacity for pay load and high accuracy [27, 28, 29]. It is worth pointing out that Stewart platform is a classic kind of parallel manipulators attracting great interest of researchers.

Especially, the study on practicability of Stewart platform is now of an increasing tendency [30, 31, 32, 33]. To solve the situation with disturbances and measurement noises in practice, Su et al. proposed a robust motion controller of Stewart platform to realize disturbance rejection while maintaining high precision in tracking control [30]. As for the disadvantages of small and

complex workplace, Gosselin and Schreiber introduced a novel mechanism of kinematically redundant parallel mechanisms based on Stewart platform [31]. This mechanism can have a large orientational workspace with singularity avoidance. In addition, to solve the problems of unpredictable actuator faults, Meng et al. proposed a novel adaptive fault-tolerant motion control scheme based on sliding mode control and offline multi-body dynamics [32]. It is worth pointing out that ZD has been successfully applied to Stewart platform by He et al. with improved performances in convergence and accuracy [33]. These efforts improve practicability of Stewart platform and expands the application of Stewart platforms.

To further reduce the consumption on computation and transmission of Stewart platform and to extend our previous research work [33] with new discoveries, in this paper, we propose a novel dynamics named event-triggered zeroing dynamics (ETZD) by incorporating event-triggered strategy to ZD. The ETZD controller of Stewart platforms is designed and analyzed. In addition, the corresponding theoretical analyses based on ZD and Lyapunov analysis are given, which guarantee the validity and effectiveness of the proposed ETZD controller. To the best of the authors' knowledge, such a motion controller incorporating event-triggered strategy to ZD, is the first attempt in Stewart platform control. Moreover, numerical experiments, including two different path tracking tasks and the comparisons with ZD controllers, substantiate the effectiveness of the proposed ETZD controller.

The remainder of this paper is organized as follows. In Section 2, the ZD controller of Stewart platform and event-triggered strategy are introduced firstly, and then ETZD controller is designed and analyzed with stability proof. In Section 3, the numerical experiments of two different shaped path tracking tasks including the comparisons with ZD controller are conducted to further illustrate the effectiveness of ETZD controller. Section 4 concluded this paper with final remarks. Before ending this introductory section, it is worth pointing out the main contributions of this paper as follows.

1) This work is the first attempt to propose and investigate ETZD. Inheriting the advantage of ZD in convergence and accuracy, ETZD further reduces computational and communicational consumption significantly.

2) A motion controller of Stewart platform is designed based on ETZD. The validity and effectiveness of the proposed ETZD controller is analyzed.

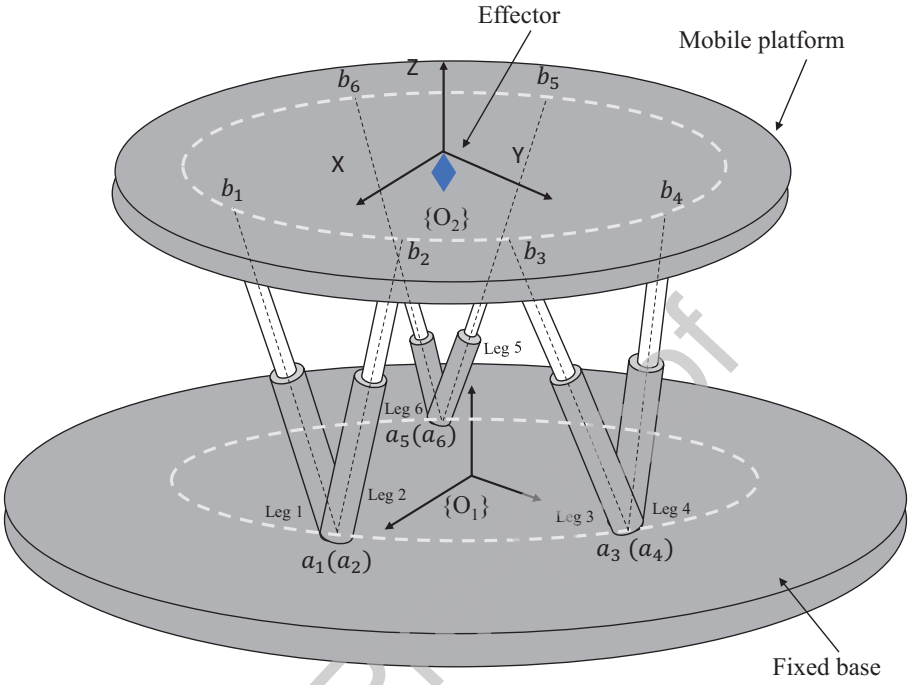

Figure 1: The model of Stewart platform.

3) Numerical experiments of two different path tracking tasks including the comparisons with traditional ZD controller further illustrate the effectiveness of the proposed ETZD controller.

2. Design and analysis of ETZD controller of Stewart platform

In this section, the preliminary knowledge of Stewart platform and ZD is firstly introduced for the design of ZD controller. Then, by incorporating event-triggered strategy, ETZD controller of Stewart platform is proposed and analyzed. The stability of ETZD controller is proved via ZD and Lyapunov analysis.

2.1. ZD controller of Stewart platform

Firstly, for better understanding of the structure and mechanism of Stewart platform, a simplified schematic model of it is shown in Figure 1. Besides,

Notation	Explanation
$\boldsymbol{r}_{\mathrm{a}}$	Actual Cartesian-position variable of effector
$\boldsymbol{r}_{\mathrm{d}}$	Desired Cartesian-position variable of effector
$\boldsymbol{l}_i$	ith prismatic joint (leg) vector, $i = 1, 2, \cdots, 6$
$\bar{\boldsymbol{l}}_i$	ith prismatic joint (leg) length, $i = 1, 2, \cdots, 6$
$A(\bar{\boldsymbol{l}})$	Coefficient matrix of the IK of Stewart platform
λ	Parameter chosen for the ZD design formula
γ	Parameter chosen for the trigger function
$\boldsymbol{q}$	Euler angles of the mobile platform
$\boldsymbol{c}$	Global coordinate of the zero point of the mobile platform

Table 1: Explanations of the frequently-used notations.

for easier understanding of the variables encountered in the ensuring content, the modeling process of the kinematics of Stewart platform is given in the Appendix [27, 33] with the frequently-used notations explained in Table 1. Note that the effector of the robot is seen as the central point of the mobile platform.

To obtain the ZD controller of Stewart platforms, we firstly construct an error vector $\boldsymbol{e}(t) = \boldsymbol{r}_{\mathrm{d}}(t) - \boldsymbol{r}_{\mathrm{a}}(t) \in \mathbb{R}^6$ between the desired pose $\boldsymbol{r}_{\mathrm{d}}(t) \in \mathbb{R}^6$ and the actual pose $\boldsymbol{r}_{\mathrm{a}}(t) \in \mathbb{R}^6$ of the effector, where t refers to the time. Note that $\boldsymbol{r}_{\mathrm{d}}(t)$, $\boldsymbol{r}_{\mathrm{a}}(t)$ and $\boldsymbol{e}(t)$ are time-varying and the pose vector consists of the position and orientation of the effector. Then, the time derivative of the error vector $\boldsymbol{e}(t)$ can be calculated as $\dot{\boldsymbol{e}}(t) = \dot{\boldsymbol{r}}_{\mathrm{d}}(t) - \dot{\boldsymbol{r}}_{\mathrm{a}}(t) \in \mathbb{R}^6$, where $\dot{\boldsymbol{r}}_{\mathrm{d}}(t)$ and $\dot{\boldsymbol{r}}_{\mathrm{a}}(t)$ refer to the time derivative of desired and actual pose trajectories.

Based on the definition of error vector and the expression of its time derivative, ZD design formula, i.e.,

$$\dot{\boldsymbol{e}}(t) + \lambda \boldsymbol{e}(t) = 0,$$

can be reformulated as

$$\dot{\boldsymbol{r}}_{\mathrm{a}}(t) = \dot{\boldsymbol{r}}_{\mathrm{d}}(t) + \lambda(\boldsymbol{r}_{\mathrm{d}}(t) - \boldsymbol{r}_{\mathrm{a}}(t)). \tag{1}$$

Then, by combining (1) and the inverse kinematics (IK) at velocity level of Stewart platforms [27, 33], i.e.,

$$\dot{\bar{\boldsymbol{l}}}(t) = A(\bar{\boldsymbol{l}})\dot{\boldsymbol{r}}_{\mathrm{a}}(t),$$

the ZD controller of Stewart platforms at velocity level can be obtained as

$$\boldsymbol{u}(t) = \dot{\bar{\boldsymbol{l}}}(t) = A(\bar{\boldsymbol{l}})(\dot{\boldsymbol{r}}_{\mathrm{d}}(t) + \lambda(\boldsymbol{r}_{\mathrm{d}}(t) - \boldsymbol{r}_{\mathrm{a}}(t))), \tag{2}$$

where $\boldsymbol{u}(t)$ refers to the control input of Stewart platforms, i.e., the velocity vector of six prismatic joints $\dot{\bar{\boldsymbol{l}}}(t)$. Note that $\lambda \in \mathbb{R}^+$ is a user-defined parameter in ZD determining the convergence rate and $A(\bar{\boldsymbol{l}}) \in \mathbb{R}^{6\times 6}$ refers to the coefficient matrix calculated from the state of Stewart platforms (i.e., the length vector of six prismatic joints $\bar{\boldsymbol{l}}(t)$). About the ZD controller (2), we have the following theoretical result.

Theorem 1 (ZD Controller Convergence). *For a Stewart platform controlled by ZD controller (2), starting from any initial pose $\boldsymbol{r}_{\mathrm{a}}(0)$, the actual pose $\boldsymbol{r}_{\mathrm{a}}(t)$ is globally and exponentially convergent to the desired pose $\boldsymbol{r}_{\mathrm{d}}(t)$ with convergence rate $\lambda > 0$.*

Proof. For ZD controller (2), the exponential convergence is proved as follows. When $\boldsymbol{u}(t)$ is applied to Stewart platform, the actual pose can be obtained via the forward kinematics (i.e., $\dot{\boldsymbol{r}}_{\mathrm{a}}(t) = A^{-1}(\bar{\boldsymbol{l}})\dot{\bar{\boldsymbol{l}}}(t)$, where $A^{-1}(\bar{\boldsymbol{l}})$ is the inverse matrix of $A(\bar{\boldsymbol{l}})$):

$$\begin{aligned}\dot{\boldsymbol{r}}_{\mathrm{a}}(t) &= A^{-1}(\bar{\boldsymbol{l}})\boldsymbol{u}(t)\\ &= A^{-1}(\bar{\boldsymbol{l}})A(\bar{\boldsymbol{l}})(\dot{\boldsymbol{r}}_{\mathrm{d}} + \lambda(\boldsymbol{r}_{\mathrm{d}}(t) - \boldsymbol{r}_{\mathrm{a}}(t)))\\ &= \dot{\boldsymbol{r}}_{\mathrm{d}}(t) + \lambda(\boldsymbol{r}_{\mathrm{d}}(t) - \boldsymbol{r}_{\mathrm{a}}(t)),\end{aligned}$$

which is exactly the transformation of ZD, i.e., (1). As investigated before [1, 2], the satisfaction of ZD guarantees the exponential rate of error convergence:

$$\boldsymbol{e}(t) = \boldsymbol{e}(0)\exp(-\lambda t),$$

which means

$$\lim_{t\to\infty} \boldsymbol{e}(t) = \lim_{t\to\infty} \boldsymbol{e}(0)\exp(-\lambda t) = 0. \tag{3}$$

The above equation (3) indicates that the actual pose $\boldsymbol{r}_{\mathrm{a}}(t)$ is globally and exponentially convergent to desired pose $\boldsymbol{r}_{\mathrm{d}}(t)$ with convergence rate $\lambda > 0$, as time t goes on (and the system enters its steady state). The proof of the theorem is thus completed. □

2.2. ETZD controller of Stewart platform

In this part, we extend the ZD controller (2) described by continuous-time control update to one with event-triggered control update by proposing the novel ETZD controller.

Firstly, a Lyapunov function is introduced:

$$V(\boldsymbol{e}) = \frac{\boldsymbol{e}^{\mathrm{T}}(t)\boldsymbol{e}(t)}{2} \in \mathbb{R},$$

where $\boldsymbol{e}(t)$ refers to the same meaning as mentioned before. It is worth pointing out that the Lyapunov function $V(\boldsymbol{e})$ is positive definite, because $V(\boldsymbol{e}) > 0$ for all $\boldsymbol{e}(t) \neq 0$ and $V(\boldsymbol{e}) = 0$ if and only if $\boldsymbol{e}(t) = 0$. Besides, $\dot{V}(\boldsymbol{e})$ refers to the corresponding time derivative of the Lyapunov function $V(\boldsymbol{e})$, i.e., $\dot{V}(\boldsymbol{e}) = \boldsymbol{e}^{\mathrm{T}}(t)\dot{\boldsymbol{e}}(t) \in \mathbb{R}$. Furthermore, an event-triggered function is constructed based on $V(\boldsymbol{e})$ and $\dot{V}(\boldsymbol{e})$:

$$J(V, \dot{V}) = \dot{V}(\boldsymbol{e}) + \gamma V(\boldsymbol{e}) \in \mathbb{R}, \tag{4}$$

where γ is a self-defined parameter being greater than 0. Then, the ETZD controller is proposed based on (4) as follows:

$$\boldsymbol{u}(t) = \dot{\bar{\boldsymbol{l}}}(t) = \begin{cases} A(\bar{\boldsymbol{l}})(\dot{\boldsymbol{r}}_{\mathrm{d}}(t) + \lambda(\boldsymbol{r}_{\mathrm{d}}(t) - \boldsymbol{r}_{\mathrm{a}}(t))) & \text{if } J(V, \dot{V}) > 0, \\ \text{last input} & \text{if } J(V, \dot{V}) \leq 0. \end{cases} \tag{5}$$

About the ETZD controller (5), we have the following theoretical result.

Theorem 2 (ETZD Controller Convergence). *For a Stewart platform controlled by ETZD controller (5), starting from any initial pose $\boldsymbol{r}_{\mathrm{a}}(0)$, the actual pose $\boldsymbol{r}_{\mathrm{a}}(t)$ is globally convergent to the desired pose $\boldsymbol{r}_{\mathrm{d}}(t)$.*

Proof. This proof is divided into two parts according to the value of the event-triggered function $J(V, \dot{V})$.

- $J(V, \dot{V}) > 0$

  The first part concerns the situation of $J(V, \dot{V}) > 0$. Note that, when the event-triggered function $J(V, \dot{V})$ is greater than 0, ETZD controller (5) degenerates into ZD controller (2). According to *Theorem 1*, the actual pose $\boldsymbol{r}_{\mathrm{a}}(t)$ can be convergent to desired pose $\boldsymbol{r}_{\mathrm{d}}(t)$ globally and exponentially.

- $J(V, \dot{V}) \leq 0$

  The second part concerns the situation of $J(V, \dot{V}) \leq 0$. When the event-triggered function J is not greater than 0, ETZD controller (5) will maintain the last input instead of a new round of computation and transmission. Thus, substituting (4) into (5), we can have the following relationship:

$$\dot{V}(\boldsymbol{e}) + \gamma V(\boldsymbol{e}) \leq 0.$$

  According to the transitive property of inequalities, we can have a relationship $\dot{V}(\boldsymbol{e}) \leq -\gamma V(\boldsymbol{e}) \leq 0$. It is worth pointing out that $\dot{V}(\boldsymbol{e})$ is negetive definite, because $\dot{V}(\boldsymbol{e}) < 0$ for all $\boldsymbol{e}(t) \neq 0$ and $\dot{V}(\boldsymbol{e}) = 0$ if and only if $\boldsymbol{e}(t) = 0$. Besides, when $\|\boldsymbol{e}(t)\|$ approaches ∞, $V(\boldsymbol{e})$ also approaches ∞. Thus, the system equipped with ETZD controller (5) meets the condition of Lyapunov's second method for stability: $V(\boldsymbol{e})$ is positive definite, $\dot{V}(\boldsymbol{e})$ is negative definite and $\|\boldsymbol{e}(t)\| \to \infty, V(\boldsymbol{e}) \to \infty$, which means that such a system equipped with ETZD controller (5) is global asymptotic stability. The actual pose $\boldsymbol{r}_{\mathrm{a}}(t)$ is globally convergent to desired pose $\boldsymbol{r}_{\mathrm{d}}(t)$, as time t goes on (and the system enters its steady state).

In summary, whatever the value of $J(V, \dot{V})$ is, the actual pose $\boldsymbol{r}_{\mathrm{a}}(t)$ is globally convergent to desired pose $\boldsymbol{r}_{\mathrm{d}}(t)$, as time t goes on (and the system enters its steady state). The proof of the theorem is thus completed. □

Remark 1. *Suppose that t_k denotes the kth trigger instant and t_{k+1} denotes the $(k+1)$th trigger instant. When $t \in [t_k, t_{k+1})$, the ETZD control signal of a prismatic joint updated at t_k is $u_i(t_k) = c$, and the accumulated error between the control signals of the ZD controller and the ETZD controller can be defined as $\epsilon_i(t) = u_i(t) - c$. One can obtain that $\dot{\epsilon}_i(t) = \dot{u}_i(t) - dc/dt = \dot{u}_i(t)$. Besides, $\forall t \in [t_k, t_{k+1})$, we have $|d\epsilon_i/dt| = |\dot{\epsilon}_i| = |\dot{u}_i|$. Given the mechanical structure of the Stewart platform, provided that the tracking path is bounded with $\ddot{r}_{\mathrm{d}}(t)$ bounded either, $|\dot{u}_i|$ is bounded by a constant η as $|\dot{u}_i| \leq \eta$. Furthermore, it is ready to know that $\epsilon_i(t_k) = 0$ and $lim_{t \to t_{k+1}} \epsilon_i(t) = \varepsilon$, which leads to $t_{k+1} - t_k \geq |\varepsilon/\eta| > 0$ as $u_i(t_k)$ and $u_i(t_{k+1})$ are generally different, also in view of the measurement and feedback errors having their precision bound, in addition to Planck time [34]. Thus, the Zeno behavior is potentially ruled out. On the other hand, when implementing the above ETZD scheme digitally or numerically, the event triggering condition (i.e.,*

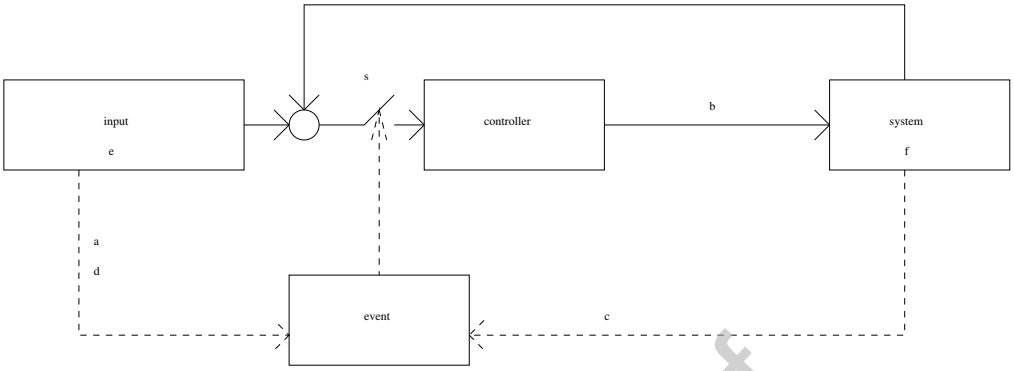

Figure 2: Diagram of ETZD controller for Stewart platform control.

the value of $J(V,\dot{V})$) is monitored with a sampling gap (i.e., a nonzero-value time discretization gap such as 5×10^{-4} s) periodically, which means that the time gap between two triggering instants is lower-bounded, excluding Zeno behavior actually.

For better understanding, the control program of ETZD is presented in Figure 2. Firstly, initialize the necessary parameters (λ and γ) and variables ($\boldsymbol{e}(t)$, $\dot{\boldsymbol{e}}(t)$, $V(\boldsymbol{e})$ and $J(V,\dot{V})$). Then, according to the given inputs (i.e., desired pose $\boldsymbol{r}_{\mathrm{d}}(t)$ and twist $\dot{\boldsymbol{r}}_{\mathrm{d}}(t)$ in Cartesian space) and the outputs measured by sensors (i.e., actual pose $\boldsymbol{r}_{\mathrm{a}}(t)$ and twist $\dot{\boldsymbol{r}}_{\mathrm{a}}(t)$ in Cartesian space), the event trigger computes the value of the event-triggered function $J(V,\dot{V})$ in real time. If $J(V,\dot{V})>0$, the corresponding switch turns on and the variables are transmitted to ZD controller. ZD controller updates the input in joint space for Stewart platform (i.e., the velocity vector $\dot{\boldsymbol{l}}(t)$ of six prismatic joints). If $J(V,\dot{V})\leq 0$, the computations and transmission are not conducted and ZD controller just maintains the last input for Stewart platforms. The Stewart platform works based on the input and updates all the variables in real time.

3. Numerical experiments

To better illustrate the effectiveness of ETZD controller, two different path tracking tasks are conducted in numerical experiments. One is the rhomboid-shaped path tracking task while the other is the ellipse-shaped path tracking task. During the experiments, a coordinate frame is established

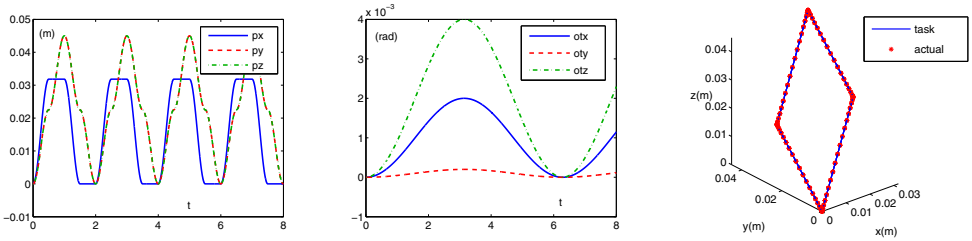

(a) Desired positions (b) Desired orientations (c) Desired and actual paths

Figure 3: Desired pose (positions and orientations), desired path and actual path of rhomboid-shaped path tracking task synthesized by ETZD controller with $\gamma = 15$ and $\lambda = 50$.

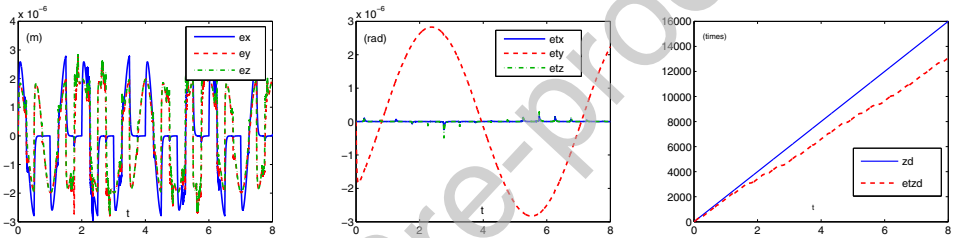

(a) Position errors (b) Orientation errors (c) Control update counts

Figure 4: Numerical experiment results of rhomboid-shaped path tracking task synthesized by ETZD controller with $\gamma = 15$ and $\lambda = 50$.

on the initial central point of the mobile platform, and the central point is also seen as the effector. Generally, the initial pose of the effector is set as $[0, 0, 0, 0, 0, 0]^{\mathrm{T}}$. The corresponding results are presented and analyzed in the following subsections. For simplicity, the pose mentioned in the ensuring discussions refers the pose of the effector's pose (i.e., the central point of the mobile platform).

3.1. Rhomboid-shaped path tracking task

This subsection concerns the rhomboid-shaped path tracking task with the duration being 8 s including 2 complete circulations. The desired pose is shown in Figure 3(a) and Figure 3(b). The desired positions in X-axis, Y-axis and Z-axis are presented as p_{X}, p_{Y} and p_{Z} respectively, while the desired orientations in three Euler angles ϕ, φ and ψ are presented as q_{ϕ}, q_{φ} and q_{ψ} respectively. Then the Stewart platform equipped with ETZD controller

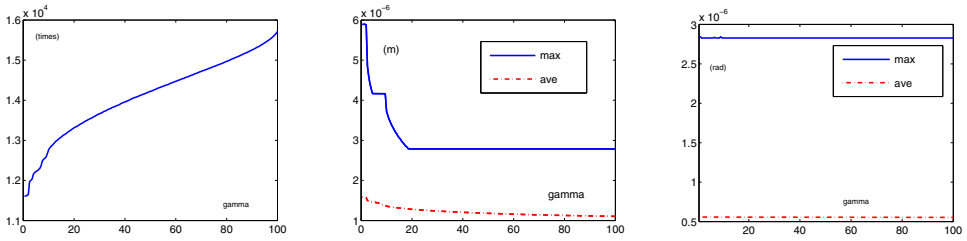

(a) Control update counts (b) MAPE and AAPE (c) MAOE and AAOE

Figure 5: Control update counts, maximum absolute pose errors (MAPE and MAOE) and average absolute pose errors (AAPE and AAOE) of rhomboid-shaped path tracking task synthesized by ETZD controller with $\lambda = 50$ and different values of $\gamma \in (0, 100]$.

($\gamma = 15$ and $\lambda = 50$) is applied to this rhomboid-shaped path tracking task. The numerical experiment results of tracking errors are presented in Figure 4(a) and Figure 4(b). As seen, the absolute values of position errors (i.e., e_{X}, e_{Y} and e_{Z}) are controlled under 3×10^{-6} m and the absolute values of orientation errors (i.e., e_{ϕ}, e_{φ} and e_{ψ}) are controlled under 3×10^{-6} rad at the same time. More intuitively, Figure 3(c) shows that the actual path almost coincides with the desired path. The above results illustrate that the Stewart platform equipped with ETZD controller successfully achieves the purpose of tracking rhomboid-shaped path with global convergence and high accuracy. It is worth pointing out that in this example the control period is 5×10^{-4} s. In the task duration, the original ZD controller needs a total of 16000 times of computation and transmission. As shown by Figure 4(c), the control update counts synthesized by ETZD controller are less than that synthesized by ZD controller. Precisely, the control update counts synthesized by ETZD controller is 13080, which is 18.25% less than that synthesized by ZD controller, which means that ETZD controller achieves high convergence and high accuracy in rhomboid-shaped path tracking task and, in the meantime, decreases consumption on computation and transmission largely.

There are two important parameters of ETZD controller (i.e., γ and λ) which have great impact on the experiment results. γ comes from the switch condition of event-triggered strategy, which is set to be greater than 0. Recall the definition of $J(V, \dot{V})$ in (4) [i.e., $J(V, \dot{V}) = \dot{V}(\boldsymbol{e}) + \gamma V(\boldsymbol{e})$]. Because $V(\boldsymbol{e})$ is a nonnegative variable, $J(V, \dot{V})$ is proportional to γ. It can be found that the bigger γ is, the easier the triggering condition is to be met. Thus, a series of numerical experiments equipped with ETZD controller with different values

of $\gamma \in (0, 100]$ and $\lambda = 50$ are conducted, of which the results including control update counts, maximum absolute pose errors and average absolute pose errors are presented in Figure 5. As verified by Figure 5(a), the control update counts increase when the value of γ increases. However, in Figure 5(b), when the value of γ increases, the maximum absolute position errors (MAPE, i.e., the maximum absolute values of position errors in three axes) and the average absolute position errors (AAPE, i.e., the average absolute values of position errors in three axes) decrease. It is worth pointing out that when the value of γ is greater than a threshold, MAPE and AAPE are shown to be stable, which indicates that a suitable value of γ can reach the optimal balance of reducing control update counts and minimizing MAPE as well as AAPE. In this case, the value of γ has little impact on the maximum absolute orientation errors (MAOE, i.e., the maximum absolute values of orientation errors in three Euler angles) and the average absolute orientation errors (AAOE, i.e., the average absolute values of orientation errors in three Euler angles).

As for the other important parameter of ETZD controller, λ has great impact on the error convergence. It is worth pointing out that λ is also an important parameter of ZD controller. Thus, a series of comparative numerical experiments are conducted to illustrate the improvements of ETZD controller. Note that γ is set to be 15 and λ is set to be in the interval of $(0, 2000]$. The corresponding results are presented in Figures 6 and 7, including the comparisons of maximum absolute pose errors (i.e., MAPE and MAOE), average absolute pose errors (i.e., AAPE and AAOE) and control update counts. As presented in Figure 6(a) and Figure 6(b), it can be found that MAPE and MAOE synthesized by ZD controller and ETZD controller all decrease in an exponential rate with the increase of the numerical value of λ.

However, MAPE and MAOE synthesized by ZD controller is smaller than those synthesized by ETZD controller, which is the sacrifice of reducing control update counts. Note that when the numerical value of λ is small enough or big enough, it is hard to find the differences in MAPE and MAOE between ZD controller and ETZD controller. Because the low error convergence rate caused by small λ means a relatively big value of $V(\boldsymbol{e})$ and the high error convergence rate caused by big λ means a relatively big value of $\dot{V}(\boldsymbol{e})$, both reasons make the event-triggered function easy to meet the switch condition. The curve synthesized by ETZD controller in Figure 7 illustrates that the small or big value of λ leads an increase of control update counts. In this

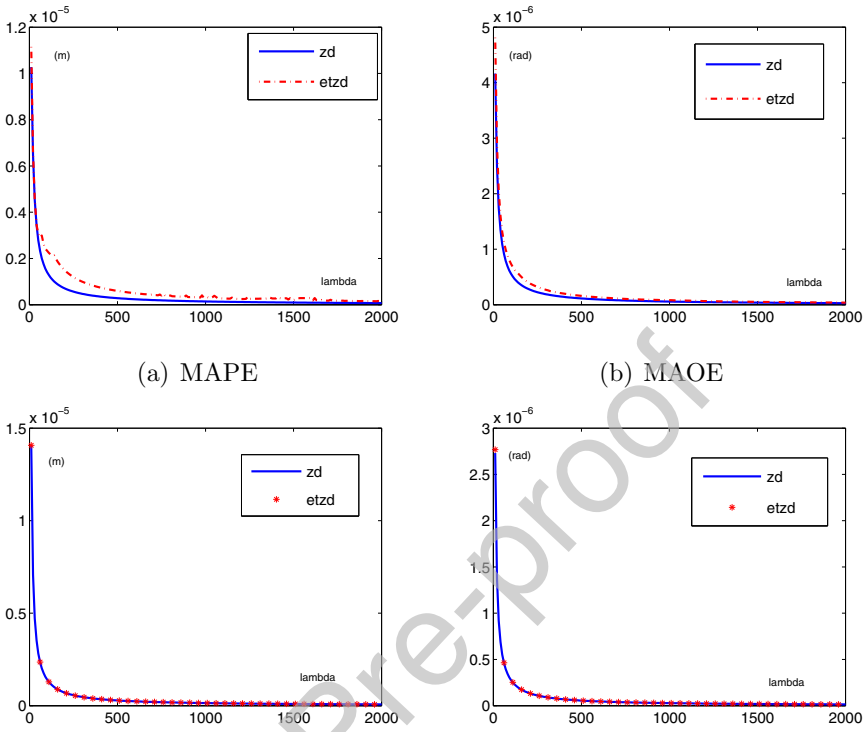

(a) MAPE (b) MAOE

(c) AAPE (d) AAOE

Figure 6: Comparisons in maximum absolute pose errors (MAPE and MAOE) and average absolute pose errors (AAPE and AAOE) between ZD controller and ETZD controller of rhomboid-shaped path tracking task with $\gamma = 15$ and different values of $\lambda \in (0, 2000]$.

example, $\lambda = 1000$ can lead to an almost lowest control update counts, and $\lambda = 1800$ can lead to smaller MAPE and MAOE but relatively higher control update counts. The determination of λ depends on the specific requirements of task. As for AAPE and AAOE presented in Figure 6(c) and Figure 6(d), it is hard to find the difference between ZD controller and ETZD controller, which means that the introduction of event-triggered strategy can maintain the overall performance of ZD controller. ETZD controller can realize the rhomboid-shaped path tracking task effectively with a good balance of obtaining high accuracy and reducing control update counts.

Table 2: Performances of ZD and ETZD controllers for rhomboid-shaped path tracking task with $\gamma = 15$ and $\lambda = 50$.

Controller	ZD	ETZD
Control update counts	16000	13080
MAPE (m)	2.785563×10^{-6}	3.062545×10^{-6}
AAPE (m)	2.827976×10^{-6}	1.313731×10^{-6}
MAOE (rad)	1.088682×10^{-6}	2.827936×10^{-6}
AAOE (rad)	5.521308×10^{-7}	5.566368×10^{-7}

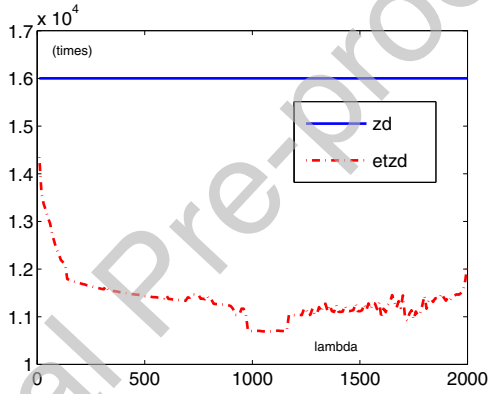

Figure 7: Comparison in control update counts between ZD controller and ETZD controller of rhomboid-shaped path tracking task with $\gamma = 15$ and different values of $\lambda \in (0, 2000]$.

3.2. Ellipse-shaped path tracking task

This subsection concerns the situation of an ellipse-shaped path tracking task with the duration being 8 s including 2 complete circulations.

Firstly, we investigate the effectiveness of the ETZD controller for this path tracking task with the parameters chosen as $\gamma = 25$ and $\lambda = 100$. The desired pose in this example is shown in Figure 8(a) and Figure 8(b). The tracking errors of this task are presented in Figure 9(a) and Figure 9(b). As seen from results, the absolute values of position errors (i.e., e_{X}, e_{Y} and e_{Z}) are controlled under 3×10^{-6} m and the absolute values of orientation errors (i.e., e_{ϕ}, e_{φ} and e_{ψ}) are controlled under 1.5×10^{-6} rad at the same time. More intuitively, Figure 8(c) shows that the actual trajectory almost

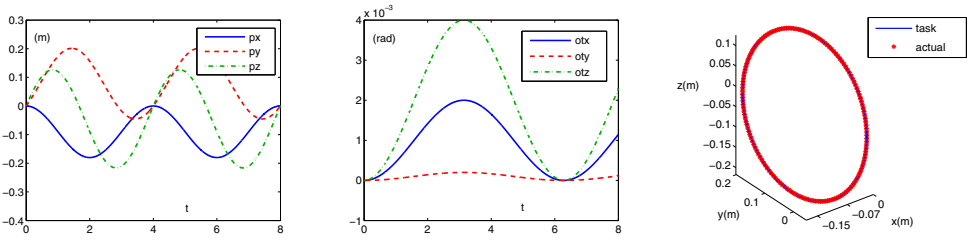

(a) Desired positions (b) Desired orientations (c) Desired and actual paths

Figure 8: Desired pose (positions and orientations), desired path and actual trajectory of ellipse-shaped path tracking task synthesized by ETZD controller with $\gamma = 25$ and $\lambda = 100$.

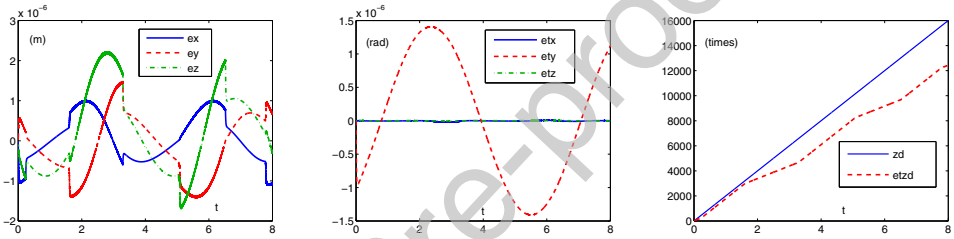

(a) Position errors (b) Orientation errors (c) Control update counts

Figure 9: Numerical experiment results of ellipse-shaped path tracking task synthesized by ETZD controller with $\gamma = 25$ and $\lambda = 100$.

coincides with the desired path. The above results illustrate that the Stewart platform equipped with ETZD controller successfully achieves the purpose of ellipse-shaped path tracking task. It is worth pointing out that, in this example, the control period is also set to be 5×10^{-4} s. As shown by Figure 9(c), the control update counts synthesized by ETZD controller are less than that synthesized by ZD controller. Precisely, the control update counts synthesized by ETZD controller is 12440, which is 77.75% of that synthesized by ZD controller, which means that ETZD controller achieves high convergence and high accuracy in ellipse-shaped path tracking task and, in the meantime, reduces the consumption of computation and transmission largely.

In the following parts, we also investigate the impact of γ and λ in a series of experiments. Firstly, a series of numerical experiments equipped with ETZD controller with different values of $\gamma \in (0, 50]$ and $\lambda = 50$ are conducted, of which the results are presented in Figure 10. Like the results

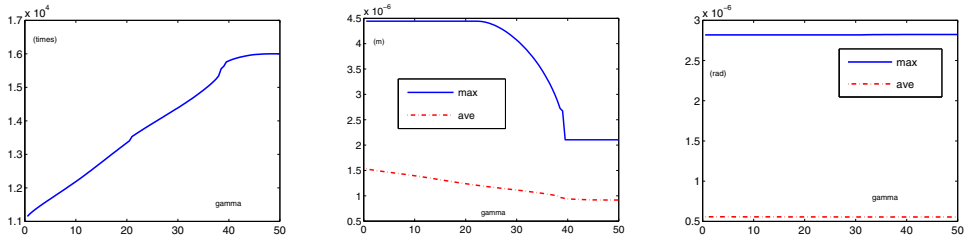

(a) Control update counts (b) MAPE and AAPE (c) MAOE and AAOE

Figure 10: Control update counts, maximum absolute pose errors (MAPE and MAOE) and average absolute pose errors (AAPE and AAOE) of ellipse-shaped path tracking task synthesized by ETZD controller with $\lambda = 50$ and different values of $\gamma \in (0, 50]$.

of rhomboid-shaped path tracking task, the control update counts increase with the increase of the numerical value of γ in Figure 10(a). Although the parameter setting is the same, there exist some differences in experiment results such as the growth rate and the specific numerical value of control update counts. These phenomena indicate that different path tracking tasks needs different values of parameters even for obtaining the same performance. As presented in Figure 10(b), when the numerical value of γ increases, MAPE and AAPE decrease but with different growth rates compared with those of rhomboid-shaped path tracking task. Similar to the results in Example 1, when the value of γ is greater than a threshold, MAPE and AAPE are shown to be stable, which indicates that a suitable numerical value of γ can reach the optimal balance of reducing control update counts and minimizing MAPE as well as AAPE. As observed in Figure 10(c), the numerical value of γ also has limited impact on MAOE and AAOE.

As for the other important parameter λ of ETZD controller, there exist similarities and differences between ellipse-shaped and rhomboid-shaped path tracking tasks. The experiment results of the comparative numerical experiments with $\gamma = 25$ and different numerical values of $\lambda \in (0, 2500]$ are presented in Figures 11 and 12, including the comparisons of MAPE, MAOE, AAPE, AAOE and control update counts. As for MAPE and MAOE, from Figure 11(a) and Figure 11(b), the similarities can be found that MAPE and MAOE synthesized by ZD controller and ETZD controller all decrease in an exponential rate with the increase of the numerical value of λ. In addition, MAPE and MAOE synthesized by ZD controller is also a little smaller than those synthesized by ETZD controller due to the sacrifice of reducing control

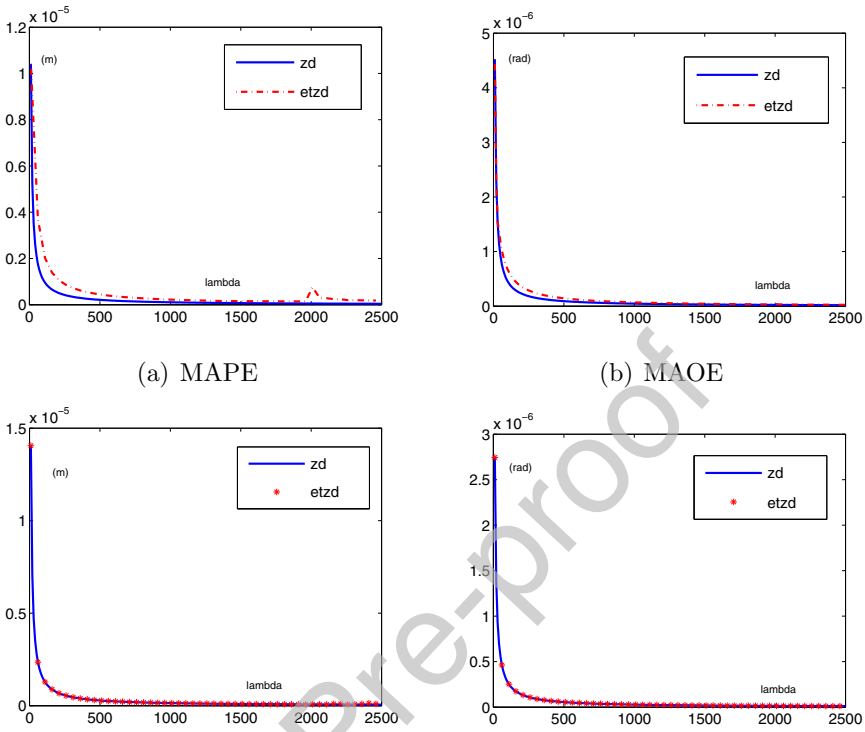

(a) MAPE (b) MAOE

(c) AAPE (d) AAOE

Figure 11: Comparisons in maximum absolute pose errors (MAPE and MAOE) and average absolute pose errors (AAPE and AAOE) between ZD controller and ETZD controller of ellipse-shaped path tracking task with $\gamma = 25$ and different values of $\lambda \in (0, 2500]$.

update counts. Note that when the value of λ is small enough or big enough, it is hard to find the differences in MAPE and MAOE between ZD controller and ETZD controller. The curve synthesized by ETZD controller in Figure 12 illustrates that the small or big value of λ leads an increase of control update counts. However, in this example, the rate of change is very different from that presented in Figure 7. Furthermore, $\lambda = 2000$ is the point that can lead to an almost lowest control update counts, and $\lambda = 1960$ is the point that can reach a great balance of MAPE, MAOE and control update counts. The above changes illustrate that the determination of λ depends on the requirements of specific tasks. As for AAPE and AAOE presented in Figure 11(c) and Figure 11(d), it is difficult to find the difference between ZD controller and ETZD controller, which means that the introduction of event-

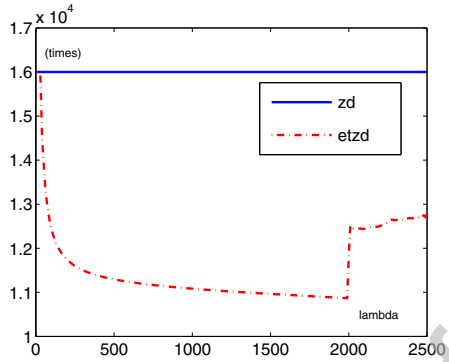

Figure 12: Comparison in control update counts between ZD controller and ETZD controller of ellipse-shaped path tracking task with $\gamma = 25$ and different values of $\lambda \in (0, 2500]$.

triggered strategy can maintain the overall performance of ZD. In summary, ETZD controller can realize the ellipse-shaped path tracking task effectively with a good balance of obtaining convergence and accuracy, and can reduce control update counts compared to ZD controller.

4. Conclusion

By incorporating the event-triggered strategy and zeroing dynamics (ZD), a novel dynamics called event-triggered zeroing dynamics (ETZD) has been proposed and investigated. The introduction of event-triggered strategy significantly reduces computational and transmission consumption and clearly outperforms conventional ZD. Further, ETZD has been employed for the motion control of Stewart platforms. The stability of the motion controller has been presented and analyzed with Lyapunov analysis. Two different shaped path tracking tasks equipped with ETZD controller illustrate its advantage in convergence, accuracy and practicability. As a final remark of this paper, to the best of our knowledge, this is the first attempt to combine event-triggered scheme and zeroing dynamics, which extends the theoretical studies on zeroing dynamics with a concrete example of parallel robot control showing the power of this approach. Also, in realistic applications, as the physical constraints of robot systems are inevitable, investigating the ETZD scheme to deal with control problems with physical restrictions is a direction worth exploring in the future researches.

Appendix: Modeling process for Stewart platform

For the Stewart platform robot system, the mobile platform is connected to the fixed base through six prismatic joints (or say, legs), which can be extended and contracted in a specific direction. Thus, the end-effecter on the mobile platform can be controlled by adjusting the length of the prismatic joints. The modeling process is recapped as follows [27, 33].

Establish the global coordinate frame $\{O_1\}$ on the fixed base with the central point being the origin. Suppose that the position in global coordinate of the ith connection point on the fixed base is $\boldsymbol{a}_i \in \mathbb{R}^3$, the position in global coordinate of the ith connection point on the mobile platform is $\boldsymbol{b}_i \in \mathbb{R}^3$ and the central point of the mobile platform in global coordinate is represented by $\boldsymbol{c} \in \mathbb{R}^3$.

Note that $^{\mathrm{T}}$ denotes the transpose of a vector or matrix and $i = 1, 2, \cdots, 6$. Accordingly, the ith prismatic joint vector is expressed as $\boldsymbol{l}_i = \boldsymbol{b}_i - \boldsymbol{a}_i \in \mathbb{R}^3$. In terms of the mobile platform, establish the platform coordinate frame $\{O_2\}$ with the central point being the origin.

Thereinto, for an arbitrary point p' in platform coordinate frame, one can find its corresponding point p in the global coordinate through the following relationship:

$$p = \boldsymbol{c} + Tp',$$

where $\boldsymbol{c}$ is the global coordinate of the zero point in the platform coordinate and T is the rotational matrix defined by the three Euler angles $q = [q_\phi, q_\varphi, q_\psi]^{\mathrm{T}}$, i.e., the rotation angles that the mobile platform rotates around X, Y and Z axes of $\{O_1\}$, as

$$T = \begin{bmatrix} \cos q_\psi & -\sin q_\psi & 0 \\ \sin q_\psi & \cos q_\psi & 0 \\ 0 & 0 & 1 \end{bmatrix} \begin{bmatrix} \cos q_\varphi & 0 & \sin q_\varphi \\ 0 & 1 & 0 \\ -\sin q_\varphi & 0 & \cos q_\varphi \end{bmatrix} \begin{bmatrix} 1 & 0 & 0 \\ 0 & \cos q_\phi & -\sin q_\phi \\ 0 & \sin q_\phi & \cos q_\phi \end{bmatrix}.$$

Furthermore, the vector of the ith prismatic joints can be rewritten as

$$\boldsymbol{l}_i = \boldsymbol{c} + T\boldsymbol{b}_i' - \boldsymbol{a}_i.$$

For the ith prismatic joint of the robot platform, we define $\bar{\boldsymbol{l}}_i = ||\boldsymbol{l}_i|| \in \mathbb{R}$ as the length of it. Accordingly, the following equation can be obtained.

$$\bar{\boldsymbol{l}}_i^2 = (\boldsymbol{c} + T\boldsymbol{b}_i' - \boldsymbol{a}_i)^{\mathrm{T}}(\boldsymbol{c} + T\boldsymbol{b}_i' - \boldsymbol{a}_i).$$

By computing the time derivative on both sides of the above equation, the velocity level relation of Stewart platform can be obtained as

$$\begin{aligned}\bar{\boldsymbol{l}}_i\dot{\bar{\boldsymbol{l}}}_i &= (\boldsymbol{c}+T\boldsymbol{b}_i'-\boldsymbol{a}_i)^{\mathrm{T}}(\dot{\boldsymbol{c}}+\dot{T}\boldsymbol{b}_i'+T\dot{\boldsymbol{b}}_i'-\dot{\boldsymbol{a}}_i)\\ &= (\boldsymbol{c}+T\boldsymbol{b}_i'-\boldsymbol{a}_i)^{\mathrm{T}}(\dot{\boldsymbol{c}}+\dot{T}\boldsymbol{b}_i').\end{aligned} \tag{6}$$

According to the property of the time derivative of transformation matrix $\dot{T}$, i.e.,

$$\dot{T} = \begin{bmatrix} 0 & -\dot{q}_\psi & \dot{q}_\varphi \\ \dot{q}_\psi & 0 & -\dot{q}_\phi \\ -\dot{q}_\varphi & \dot{q}_\phi & 0 \end{bmatrix} T = \dot{\boldsymbol{q}} \times T,$$

with $\times$ denoting the cross product between vectors and matrices, equation (6) can be rewritten as

$$\begin{aligned}\bar{\boldsymbol{l}}_i\dot{\bar{\boldsymbol{l}}}_i &= \boldsymbol{l}_i^{\mathrm{T}}(\dot{\boldsymbol{c}}+\dot{\boldsymbol{q}}\times T\boldsymbol{b}_i') = \boldsymbol{l}_i^{\mathrm{T}}\dot{\boldsymbol{c}}+(\dot{\boldsymbol{q}}\times(T\boldsymbol{b}_i'))^{\mathrm{T}}\boldsymbol{l}_i\\ &= \boldsymbol{l}_i^{\mathrm{T}}\dot{\boldsymbol{c}}+(T\boldsymbol{b}_i'\times\boldsymbol{l}_i)^{\mathrm{T}}\dot{\boldsymbol{q}}.\end{aligned} \tag{7}$$

By combining vectors $\boldsymbol{c}\in\mathbb{R}^3$ and $\boldsymbol{q}\in\mathbb{R}^3$, a new pose vector $\boldsymbol{r}\in\mathbb{R}^6$ is obtained, which can denote the position and orientation of the central point of the mobile platform. Furthermore, as the length of the prismatic joints of between the base and the mobile platform is always positive, the inverse kinematic of a specific joint of the Stewart platform is obtained as

$$\dot{\bar{\boldsymbol{l}}}_i = \begin{bmatrix} \boldsymbol{l}_i^{\mathrm{T}}/\bar{\boldsymbol{l}}_i, & (T\boldsymbol{b}_i'\times\boldsymbol{l}_i)^{\mathrm{T}}/\bar{\boldsymbol{l}}_i \end{bmatrix}\begin{bmatrix} \dot{\boldsymbol{c}} \\ \dot{\boldsymbol{q}} \end{bmatrix} = \begin{bmatrix} \boldsymbol{l}_i^{\mathrm{T}}/\bar{\boldsymbol{l}}_i, & (T\boldsymbol{b}_i'\times\boldsymbol{l}_i)^{\mathrm{T}}/\bar{\boldsymbol{l}}_i \end{bmatrix}\dot{\boldsymbol{r}}. \tag{8}$$

Considering all six legs of the Stewart platform, we have its compact matrix-form inverse kinematic of velocity level as follows:

$$\dot{\bar{\boldsymbol{l}}} = A(\bar{\boldsymbol{l}})\dot{\boldsymbol{r}}, \tag{9}$$

where

$$A(\bar{\boldsymbol{l}}) = \begin{bmatrix} \boldsymbol{l}_1^{\mathrm{T}}/\bar{\boldsymbol{l}}_1, & (T\boldsymbol{b}_1'\times\boldsymbol{l}_1)^{\mathrm{T}}/\bar{\boldsymbol{l}}_1 \\ \boldsymbol{l}_2^{\mathrm{T}}/\bar{\boldsymbol{l}}_2, & (T\boldsymbol{b}_2'\times\boldsymbol{l}_2)^{\mathrm{T}}/\bar{\boldsymbol{l}}_2 \\ \cdots, & \cdots \\ \boldsymbol{l}_6^{\mathrm{T}}/\bar{\boldsymbol{l}}_6, & (T\boldsymbol{b}_6'\times\boldsymbol{l}_6)^{\mathrm{T}}/\bar{\boldsymbol{l}}_6 \end{bmatrix}\in\mathbb{R}^{6\times 6}.$$

References

[1] Y. Zhang, C. Yi, Zhang Neural Networks and Neural-Dynamic Method. Nova, New York, 2011.

[2] Y. Zhang, L. Xiao, Z. Xiao, M. Mao, Zeroing Dynamics, Gradient Dynamics, and Newton Iterations. CRC Press, Boca Raton, 2015.

[3] D. Guo, Z. Nie, L. Yan, The application of noise-tolerant ZD design formula to robots' kinematic control via time-varying nonlinear equations solving, IEEE Trans. Syst., Man, Cybern. Syst. 48 (12) (2018) 2188–2197.

[4] M. D. Petkovic, P. S. Stanimirovic, V. N. Katsikis, Modified discrete iterations for computing the inverse and pseudoinverse of the time-varying matrix, Neurocomputing 289 (2018) 155–165.

[5] L. Xiao, Accelerating a recurrent neural network to finite-time convergence using a new design formula and its application to time-varying matrix square root, J. Frankl. Inst. 354 (2017) 5667–5677.

[6] L. Xu, Application of the Newton iteration algorithm to the parameter estimation for dynamical systems, J. Comput. Appl. Math. 288 (2015) 33–43.

[7] P. Benner, P. Kurschner, J. Saak, Low-rank Newton-ADI methods for large nonsymmetric algebraic Riccati equations, J. Frankl. Inst. 353 (2016) 1147–1167.

[8] Y. Zhang, X. Yu, Y. Yin, C. Peng, Z. Fan, Singularity-conquering ZG controllers of z2g1 type for tracking control of the IPC system, Int. J. Control 87 (9) (2014) 1729–1746.

[9] Y. Zhang, Z. Xiao, D. Guo, M. Mao, Y. Yin, Singularity-conquering tracking control of a class of chaotic systems using Zhang-gradient dynamics, IET Control Theory Appl. 9 (6) (2015) 871–881.

[10] B. Liao, Q. Xiang, Discrete-time noise-suppressing Zhang neural network for dynamic quadratic programming with application to manipulators, Eng. Lett. 25 (2017) 431–437.

[11] Q. Ma, S. Qin, T. Jin, Complex Zhang neural networks for complex-variable dynamic quadratic programming, Neurocomputing 330 (2019) 56–69.

[12] P. Miao, Y. Shen, Y. Huang, Y. Wang, Solving time-varying quadratic programs based on finite-time Zhang neural networks and their application to robot tracking, Neural Comput. Appl. 26 (3) (2015) 693–703.

[13] Z. Zhang, L. Kong, L. Zheng, P. Zhang, X. Qu, B. Liao, Z. Yu, Robustness analysis of a power-type varying-parameter recurrent neural network for solving time-varying QM and QP problems and applications, IEEE Trans. Syst, Man, Cybern. Syst. to be published, DOI: 10.1109/TSMC.2018.2866843

[14] D. Chen, Y. Zhang, Minimum jerk norm scheme applied to obstacle avoidance of redundant robot arm with jerk bounded and feedback control, IET Control Theory Appl. 10 (15) (2016) 1896–1903.

[15] X. Su, F. Xia, J. Liu and L. Wu, Event-triggered fuzzy control of nonlinear systems with its application to inverted pendulum systems, Automatica 94 (2018) 236–248.

[16] L. Etienne, Y. Khaled, S. Di Gennaro, J. P. Barbot, Asynchronous event-triggered observation and control of linear systems via impulsive observers, J. Frankl. Inst. 354 (2017) 372–391.

[17] M. Yu, C. Yan, C. Li, Event-triggered tracking control for couple-group multi-agent systems, J. Frankl. Inst. 354 (2017) 6152–6169.

[18] X. Tan, J. Cao, X. Li, Consensus of leader-following multiagent systems: A distributed event-triggered impulsive control strategy, IEEE Trans. Cybern. 49 (3) (2019) 792–801.

[19] Q.-Y. Fan, G.-H. Yang, Sampled-data output feedback control based on a new event-triggered control scheme, Inf. Sci. 414 (2017) 306–318.

[20] C. Pradeepa, Y. Cao, R. Murugesuc, R. Rakkiyappand, An event-triggered synchronization of semi-Markov jump neural networks with time-varying delays based on generalized free-weighting-matrix approach, Math. Comput. Simul. 121 (2019) 41–56.

[21] F. Wang, M. Hou, X. Gao, G. Duan, Event-triggered backstepping control for attitude stabilization of spacecraft, J. Frankl. Inst. 356 (2019) 9474–9501.

[22] Z. Li, J. Deng, R. Lu, Y. Xu, J. Bai, C. Y. Su, Trajectory-tracking control of mobile robot systems incorporating neural-dynamic optimized model predictive approach, IEEE Trans. Syst., Man, Cybern. A, Syst. 46 (6) (2016) 740–749.

[23] Z. Zhang, L. Zheng, J. Yu, Y. Li, Z. Yu, Three recurrent neural networks and three numerical methods for solving repetitive motion planning scheme of redundant robot manipulators, IEEE/ASME Trans. Mechatron. 22 (3) (2017) 1423–1434.

[24] Z. Zhang, T. Fu, Z. Yan, L. Jin, L. Xiao, Y. Sun, Z. Yu, Y. Li, A varying-parameter convergent-differential neural network for solving joint-angular-drift problems of redundant robot manipulators, IEEE/ASME Trans. Mechatron. 23 (2) (2018) 679–689.

[25] H. R. Nohooji, I. Howard, L. Cui, Neural network adaptive control design for robot manipulators under velocity constraints, J. Frankl. Inst. 355 (2018) 693–713.

[26] H. Navvabi, A. H. D. Markazi, Position control of Stewart manipulator using a new extended adaptive fuzzy sliding mode controller and observer (E-AFSMCO), J. Frankl. Inst. 355 (2018) 2583–2609.

[27] A. M. Mohammed, S. Li, Dynamic neural networks for kinematic redundancy resolution of parallel Stewart platforms, IEEE Trans. Cybern. 46 (7) (2016) 1538-1550.

[28] T. D. Le, H.-J. Kang, An adaptive tracking controller for parallel robotic manipulators based on fully tuned radial basic function networks, Neurocomputing 137 (2014) 12–23.

[29] Y. Patel, P. George, Parallel manipulators applications - a survey, Mod. Mech. Eng. 2 (2012) 57–64.

[30] Y. X. Su, B. Y. Duan, C. H. Zheng, Y. F. Zhang, G. D. Chen, J. W. Mi, Disturbance-rejection high-precision motion control of a Stewart platform, IEEE Trans. Control Syst. Technol. 12 (3) (2004) 364–374.

[31] C. Gosselin, L. T. Schreiber, Kinematically redundant spatial parallel mechanisms for singularity avoidance and large orientational workspace, IEEE Trans. Robot. 32 (2) (2016) 286–300.

[32] Q. Meng, T. Zhang, X. Gao, J. Y. Song, Adaptive sliding mode fault-tolerant control of the uncertain Stewart platform based on offline multi-body dynamics, IEEE/ASME Trans. Mechatron. 19 (2014) 82–894.

[33] Y. Zhang, L. He, S. Li, D. Chen, Y. Ding, Zeroing dynamics based motion control scheme for parallel manipulators, Electron. Lett. 53 (2017) 74–75.

[34] M. Ossiander, F. Siegrist, V. Shirvanyan, R. Pazourek, A. Sommer, T. Latka, A. Guggenmos, S. Nagele, J. Feist, J. Burgdorfer, R. Kienberger, M. Schultze, Attosecond correlation dynamics. Nature Phys. 13 (2017) 280–285.

Declaration of Interest Statement

I am writing to declare that this work has no conflict of interests with anyone, to the best of our knowledge.

All Authors